



OPEN ACCESS

EDITED BY

Zizheng Guo,
Hebei University of Technology, China

REVIEWED BY

Alexey N. Beskopylny,
Don State Technical University, Russia
Jun He,
Hebei University of Technology, China

*CORRESPONDENCE

Zhenshan Wang,
✉ wangdayuwang@126.com

SPECIALTY SECTION

This article was submitted to Geohazards and Georisks, a section of the journal Frontiers in Earth Science

RECEIVED 24 November 2022

ACCEPTED 07 February 2023

PUBLISHED 17 February 2023

CITATION

Wei J, Wang Z, Xu J and Jia H (2023), Study on the corrosion resistance of composite modified anti-corrosion mortar under the action of bio-organic water. *Front. Earth Sci.* 11:1106872. doi: 10.3389/feart.2023.1106872

COPYRIGHT

© 2023 Wei, Wang, Xu and Jia. This is an open-access article distributed under the terms of the [Creative Commons Attribution License \(CC BY\)](https://creativecommons.org/licenses/by/4.0/). The use, distribution or reproduction in other forums is permitted, provided the original author(s) and the copyright owner(s) are credited and that the original publication in this journal is cited, in accordance with accepted academic practice. No use, distribution or reproduction is permitted which does not comply with these terms.

Study on the corrosion resistance of composite modified anti-corrosion mortar under the action of bio-organic water

Jun Wei¹, Zhenshan Wang^{2*}, Jibin Xu² and Haiqin Jia²

¹School of Civil Engineering, Suzhou University of Science and Technology, Suzhou, China, ²School of Civil Engineering and Architecture, Xi'an University of Technology, Xi'an, China

The concrete structure will be seriously eroded in a sewage environment, causing substantial economic losses. Therefore, it is of great significance to repair the existing corrosion structure. In order to quickly restore the mechanical properties and enhance the durability performance of eroded concrete structures, this paper develops a new composite high-durability mortar by adding polypropylene fibers, basalt fibers and impermeable agents, which can achieve the dual requirements of structural repair and protection. For the new material, this test set up a total of five groups of mixing ratios. This test analyzed the water absorption, mass loss rate, compressive strength and other performance indicators of the test block in the corrosive environment, and scanned and studied the microstructure of each mortar test block after corrosion. It was found that the new anti-corrosion mortar has relatively less crystallization, dense internal structure, and significantly lighter erosion. From the mechanical properties, the strength of ordinary polymer mortar after erosion decreased by 6%; high-durability mortar instead improved the strength by nearly 20%, showing better resistance to erosion. Taken together, the use of mineral dopants and water repellents can effectively enhance the strength and corrosion resistance of mortar, and the cost is low, with good prospects for engineering applications.

KEYWORDS

mortar, sewage erosion, durability, compressive strength, erosion mechanisms

1 Introduction

With the advantages of low cost, stable performance, and convenient construction, concrete is widely used in engineering. However, the performance of concrete materials in corrosive environments will degrade significantly, causing economic losses amounting to hundreds of billions of dollars per year. As a result, there is a massive demand for repair work on corroded concrete (Schneider, 2015; Bahtli and Ozbay, 2020; Negar and Nemkumar 2021). The actual project usually uses high-performance mortar reinforcement technology for repair treatment. The repaired concrete is required to have good corrosion resistance in addition to restoring the structural load-bearing function to meet the engineering needs in corrosive environments (Xu et al., 2020). Therefore, the study of high-performance repair mortar has important practical significance for prolonging the structure's service life and predicting the material's remaining life after corrosion (Huang et al., 2020a; Guo et al., 2020; Jiang et al., 2020).

As a typical corrosive environment, sewage will produce multi-factor erosion effects such as biology and acid on the structures in service. Among them, biological acids and hydrogen sulfide produced by a large number of microorganisms in the wastewater are the leading cause of erosion (Song et al., 2018; Wang et al., 2022); Therefore, domestic and foreign scholars have conducted studies on the corrosive effects of cementitious materials in acid environments. Scholars have studied the performance of concrete under acid rain. It is found that in the early stage of acid rain erosion, the erosion depth of concrete is limited, the internal cementitious material of the structure will continue to hydrate, and the compressive strength and quality of concrete will increase. As erosion intensifies, its mechanical properties will decline (Mahdikhani et al., 2018; Ma et al., 2021). In an acidic environment, cementitious materials produce large mass losses and generate erosive substances such as gypsum and ettringite, which continuously fill the pores with increasing erosion, causing the material to crack and leading to severe degradation of mechanical properties (Nehdi et al., 2014; Izquierdo et al., 2016; Kallel et al., 2016). The corrosion effects of H₂S and biological sulfuric acid generated by microbial redox on structures have attracted the attention of many scholars. Li et al. (2019) studied the relationship between H₂S concentration and corrosion of cement-based materials. It was found that the oxidation rate of chemical sulfides was exponentially related to the concentration of hydrogen sulfide. The concentration of H₂S in a humid environment is proportional to the degree of concrete deterioration. H₂S will increase the rate of microbial metabolism and acid production. However, the high concentration of H₂S weakened the oxidation activity of sulfide, and the sulfide absorption on the material surface showed a trend of increasing and then decreasing (Jensen et al., 2011; Sun et al., 2019). Huber et al. (2016) studied the effect of chemical sulfuric acid and biological sulfuric acid corrosion on the degradation performance of cement-based materials. The results show no significant difference between the two kinds of acid erosion, and the degree of damage depends on the pH value. The lower the pH value, the more serious the corrosion of cement-based materials.

In addition, some scholars have found that mineral admixtures such as silica fume and slag powder are added to concrete, and the mass loss rate of materials decreases with the increase of mineral admixtures. Mineral admixtures can improve the corrosion resistance of concrete and prolong the service life (Noeiaghahi et al., 2017; Łukowski and Dębska, 2019; Wang et al., 2020; Pandey and Kumar 2020; Wu et al., 2020). The right amount of admixture can reduce the porosity, average pore size, and maximum pore size of concrete. Macroporous and capillary pores are obviously reduced and gradually transformed into gel pores (<10 nm) and transition pores (10–100 nm). The refinement of the pores improves the denseness of the concrete, especially the volcanic ash activity effect of silica fume, and the filling effect of the newly generated C-S-H gel and silica fume significantly reduces the porosity of the structure (Gao et al., 2022). In summary, cementitious material as an alkaline substance will significantly deteriorate regardless of the acidic conditions of liquid or gas. Adding mineral admixtures will improve its corrosion resistance to a certain extent.

As a green and highly durable material, basalt fiber can significantly improve the corrosion resistance of cement cementitious materials, and many scholars have conducted

related research. First, the mechanical properties of basalt fibers in acid and salt environments decline slowly and have excellent durability (Fiore et al., 2016; Danuta et al., 2018; Wang et al., 2018). After adding concrete, it can form a certain pulling effect in its interior and improve its mechanical properties. At the same time, the compactness and impermeability of the material are significantly improved, thereby enhancing its corrosion resistance (Elgabbas et al., 2016; Afroz et al., 2017; Ralegaonkar et al., 2018). However, the fiber content is more stringent; low content will weaken the impermeability; dosage is too high will have a more significant impact on the compactness of concrete, thereby reducing its durability. Basalt fiber dosing at 0.1% is the most economical and reasonable; too much will increase the porosity, affecting the strength of concrete and adversely affecting the durability of concrete (Wang et al., 2020; Alkharabsheh et al., 2022). When the basalt fiber admixture is 0.15%, the internal pore size of concrete decreases from greater than 100 nm to less than 20 nm. But a large amount of basalt fiber increases the porosity so that the pore size between 200 nm and 3000 nm rises significantly. When the fiber admixture is reduced to 0.05%, the concrete crack control ability becomes poor, increasing large pores, and the deterioration of the pore structure weakens the adsorption of harmful ions by the material, which will make the inhibition of chloride ion penetration effect weakened. Reasonable control of basalt fiber doping can not only control the development of cracks but also optimize the pore size distribution, increase the number of capillary pores, and block the infiltration of harmful ions (Wang et al., 2020). Reinforced concrete structures use the high durability of basalt fiber to significantly improve corrosion resistance Quagliarini et al. (Quagliarini et al., 2015) found that basalt fibers wrapped around supported concrete members in an acidic environment effectively improved the force properties after corrosion and significantly reduced the corrosion rate of the reinforcement.

It was found that porosity is an essential factor affecting cementitious materials' permeability and directly affecting their corrosion resistance (Zhang et al., 2022). In order to improve the impermeability of cement cementitious materials, some scholars have carried out related research. Adding a waterproofing agent can reduce the number of open pores in concrete, lower water absorption, and effectively improve the resistance to chloride ion diffusion (Xiang et al., 2021; Chen et al., 2022). Sodium methyl silicate in cementitious materials will form a water-repellent reticular film with low surface tension to block ion penetration, thus significantly improving the impermeability of the material (Li et al., 2022; Ma et al., 2022). Inorganic water repellents can generate insoluble colloids and swelling compound salt crystals inside the material to fill the pores and increase the material's density, improving the material's corrosion resistance. There are few studies on the corrosion resistance of cement cementitious materials with a waterproofing agent, and it is of great significance to carry out relevant research.

This paper proposes a new composite highly durable mortar based on basalt fibers, combined with organic and inorganic water repellents and mineral admixtures. The mortar test blocks with different matching ratios were eroded under a high concentration of bio-organic water environment for 240 d. The macroscopic performance, such as water absorption rate, mass loss rate and compressive strength of each mortar specimen block were observed,

TABLE 1 Artificial bio-organic water ration (unit: g).

Starch	Glucose	Peptone	Urea	Diammonium hydrogen phosphate	MgSO4	NaCl	Vitamins	Compound fertilizer
614.4	251.52	69.6	25	15	200	200	7.5	20

Note: Add 1 kg sludge and 1 kg algae-rich water per 20 kg water as the biological source.

and combined with microscopic performance indexes such as SEM electron microscopy scanning and XRD chemical composition analysis to verify the corrosion resistance of the new highly corrosion-resistant mortar. To provide technical references for the construction and rehabilitation of wastewater projects.

2 Materials

The test used P · O 42.5 ordinary Portland cement; river sand is used as fine aggregate; basalt fiber and polypropylene fiber were selected as fibers, and the optimum content was 0.1% and 0.05%, respectively. Polycarboxylic acid high-performance liquid water reducer as additive; mineral powder (S95 superfine white mineral powder), silica fume, and quartz sand were selected as mineral admixtures; other additives include titanium dioxide, sodium methyl silicate, and inorganic aluminum salt waterproofing agent.

Considering the actual living environment and the corrosion effect of microorganisms, a high-concentration organic biocorrosion solution was prepared. Configuration method: Sewer sludge impurities (under an anaerobic environment) were selected and placed in an erosion barrel as a biological source. An organic aqueous solution was configured, as shown in Table 1.

In the test, we set up five groups of ratios, S1 for double-doped fiber mortar, S2 for finished polymer mortar, and S3-S5 ratios were analyzed for the effects of sodium methyl silicate, inorganic aluminum salt water repellent; the specific ratios are shown in Table 2 Test block erosion cycle of 240 d, every 60 d to observe the macroscopic performance of each ratio water absorption rate, mass loss rate, compressive strength, etc., and combined with SEM electron microscopy scanning and The corrosion resistance of each ratio after corrosion was analyzed by combining SEM electron microscopy scanning and XRD chemical composition analysis and other microscopic indicators.

3 Test method

3.1 Mass loss rate

The specimens are subjected to different degrees of damage in the erosion solution and are accompanied by changes in mass. The determination of the mass loss rate reflects the degree of apparent damage to the test block in the erosion solution. The test blocks are dried after different cycles of erosion (until the mass of the test block is constant after drying) and then weighed and recorded. The mass loss was calculated as follows.

$$\Delta W_n = \frac{G_0 - G_n}{G_0} \times 100\%$$

where G_0 is the initial mass of mortar before erosion (g); G_n is the drying mass of mortar after n days of erosion (g).

3.2 Water absorption rate

Water absorption reflects the resistance of concrete to external water entering the concrete interior, and it is an important indicator of mortar durability. The saturation mass, drying mass, and volume of the specimens was measured by removing the specimens at the specified age, and the measurement procedure was as follows.

First, the test block was taken out of the soaking solution and dried in water until the mass was constant and then measured, and the result was its saturated mass. The volume of the test block was measured in the measuring cylinder by the drainage method to reduce the test error. Next, the test block will be put into a constant temperature drying oven for drying until the mass is stable weight, and weighing after the constant weight. The water absorption rate is calculated according to the following formula.

$$w = \frac{m_s - m_d}{m_d} \times 100\%$$

where w is the water absorption rate of mortar, m_s is the saturated mass of the corrosion specimen; m_d is the drying mass of the corrosion specimen.

3.3 Compressive strength

Compressive strength is one of the main indicators of the mechanical properties of mortar, and it can reflect the corrosion resistance of mortar in harsh environments. According to the test method of mechanical properties of ordinary concrete (GB/T50081), specimens reaching the age of erosion were subjected to axial compression tests to analyze the compressive properties of different mix ratios after erosion. To ensure the accuracy of the data, we took three test blocks for each ratio for testing. The testing machine's falling speed (0.45 mm/min) was controlled by the method of controlled displacement, and the loading was stopped after reaching 75% of the maximum bearing capacity.

3.4 SEM

The electron microscope scan can visualize the microscopic morphology of mortar and observe the damaged condition inside the mortar. The JSM-6700F* cold field emission scanning electron microscope was used for microscopic electron microscopy scanning. After sampling the mortar specimen pieces, the samples were rinsed with anhydrous ethanol and then dried and stored. The morphology could be observed by placing the models on the observation plate of the electron microscope instrument.

TABLE 2 Mortar mix ratio (unit: kg/m³).

Material type	S1	S2	S3	S4	S5	
cement	348	polymer mortar Material: Water =100:16	300	300	300	
sand	450		400	400	400	
water	106		106	106	106	
water reducing admixture	3.5		4	5.5	4.5	
slump retaining agent	1		1	1	1	
basalt fiber	1.5		1.5	1.5	1.5	
mekralon	0.6		0.6	0.6	0.6	
titanium dioxide			0.5	0.5	0.5	
mineral fines			60	60	60	
silica fume			10	10	10	
quartz sand			50	50	50	
methyl sodium silicate			0.6		0.6	
inorganic aluminum salt					6	6

3.5 XRD

X-ray diffraction allows the determination of the material composition and can reveal the hydration characteristics of mortar and its effect on strength changes at the microscopic level. Samples are taken within about 5 mm from the surface of the mortar specimen, rinsed with anhydrous ethanol, dried, and finally ground with a mortar and then sieved to produce a finer powder for storage. The test current is 40 mA, the voltage is 40 kV, and the diffraction angle scanning range is 10–60°.

4 Results and discussion

4.1 Apparent phenomena

The apparent changes of mortar under erosion are shown in Figure 1; the degree of apparent damage becomes more severe with increasing erosion cycles. After 60 days of erosion, the surfaces of S1 and S2 specimens produced many crystals with brown-black color (algae deposition). In contrast, the surfaces of S3–S5 specimens had relatively few crystals. After 240 days of erosion, S1 and S2 specimens increased crystallization, further darkening of surface color and severe erosion, while S3–S5 specimens had relatively less eroded material on the surface and lighter erosion. In general, additive materials such as mineral dopants and waterproofing agents play an active role in corrosion resistance.

4.2 Compression analysis

After the corrosion of each test block pressure analysis, it can be seen from Figure 2 that more cracks are generated on the surface of the test block and accompanied by slight surface

peeling. Among them, S1 and S2 have more cracks and are mostly penetration cracks, with the most severe damage pattern; S3–S5 produce slight bulging after being pressurized, with fine cracks mainly, and the overall damage is light. In addition, the mortar specimens did not have a large amount of shedding after compressive injury, indicating that the fibers exerted their toughening and crack-resisting effects.

4.3 SEM electron microscopy scan

4.3.1 SEM electron microscopy scan

After erosion, the pore conditions of each ratio are shown in Figure 3. It can be found that S1 and S2 have loose structures and many pores, and most of them are large pores. S3 and S5 surface pores less, mainly small and medium pores; the S4 structure is dense, some medium pores exist, and the overall performance is better, indicating that the mineral admixture and waterproofing agent can effectively fill the pores and improve the degree of compactness.

Figure 4 shows the microscopic image inside the material after 240 d of erosion. S1 and S2 specimens have internal hydrated plate fragmentation; the surface structure is loose, can be observed needle rod-like calcium aluminate crystals generated, and almost no Ca(OH)₂ observed, indicating that the internal structure of the specimen has been more severe corrosion. S3 internal surface corrosion is less than S1 and S2, did not find the existence of calcium aluminate crystals on the surface. Its hydration plate is basically complete, and some Ca(OH)₂ can be observed, indicating that the hydration products of the test block are slightly corroded. S4 in the Ca(OH)₂ crystals can be observed; the overall denser, but micro-cracks exist. S5 in the structure is dense, and the plate is continuous and complete; the surface of the specimen is less corroded, indicating that the effect of water-repellent double admixture is better than a single admixture.



FIGURE 1
Apparent phenomena.

In general, the addition of each admixture can improve the compactness of the structure and reduce porosity. Among them, sodium methyl silicate and inorganic aluminum salt waterproofing agents are better for improving compactness and corrosion resistance.

4.3.2 XRD chemical composition analysis

The XRD pattern before erosion is shown in Figure 5. The material detected in S2 is mainly calcium carbonate, and the peak is much higher than the rest of the ratios; it indicates that serious

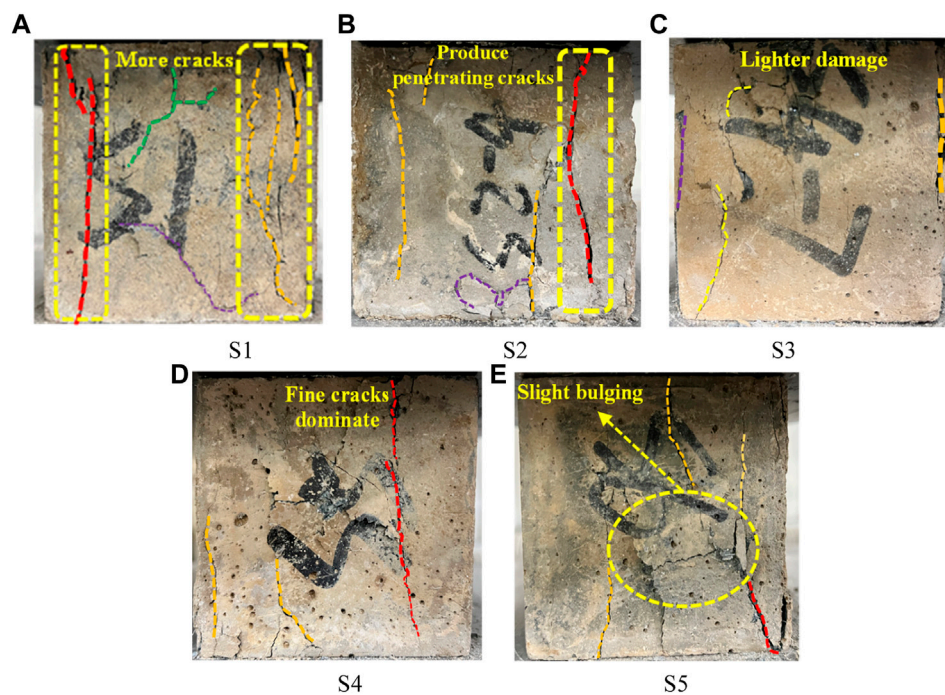


FIGURE 2

Axial compression failure pattern. (A) Axial compression failure phenomenon of S1 specimens. (B) Axial compression failure phenomenon of S2 specimens. (C) Axial compression failure phenomenon of S3 specimens. (D) Axial compression failure phenomenon of S4 specimens. (E) Axial compression failure phenomenon of S5 specimens.

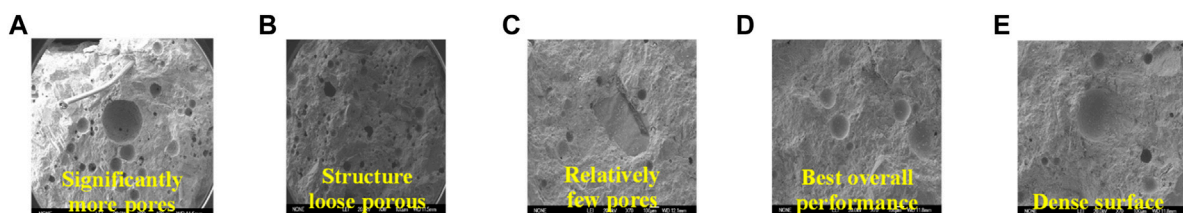


FIGURE 3

Pore status of the material after 240 d of erosion (30 \times). (A) Internal pore image of S1 specimens. (B) Internal pore image of S2 specimens. (C) Internal pore image of S3 specimens. (D) Internal pore image of S4 specimens. (E) Internal pore image of S5 specimens.

carbonization occurs inside S2, and the material deterioration will be accelerated after erosion, so the rest of the proportions except S2 are mainly analyzed.

S3 and S5 test blocks have higher SiO₂ diffraction peaks than S1. In contrast, calcium hydroxide diffraction peaks are detected more in S1 and less in the remaining ratios, indicating that SiO₂, the main component of mineral admixture, reacts with Ca(OH)₂. Higher unhydrated calcium silicate peaks were detected in S3, while silica and unhydrated calcium silicate peaks were lower in S4 and S5 than in S3. This indicates that the addition of sodium methyl silicate hinders the hydration of the cement to a certain extent. At the same time, the inorganic aluminum salt waterproofing agent makes the internal reaction of the test block more complete.

As can be seen from Figure 6, As the erosion cycle increases, the loss of Ca(OH)₂ in S1 is severe. At the same time, silica and unhydrated calcium silicate keep increasing, indicating that a large amount of damage has been generated within S1 and prevents further hydration of the cement. The new crystalline phase ettringite was detected in S1 after erosion (consistent with microscopic electron microscopy). The biological acid produced by microorganisms will react with calcium hydroxide, and the expansion substances such as gypsum and ettringite will destroy the material's internal structure and lead to the degradation of material properties. A slight decrease in the calcium hydroxide diffraction peak was found in S3-S5, but no new substances were detected. This indicates that adding each additive effectively limits

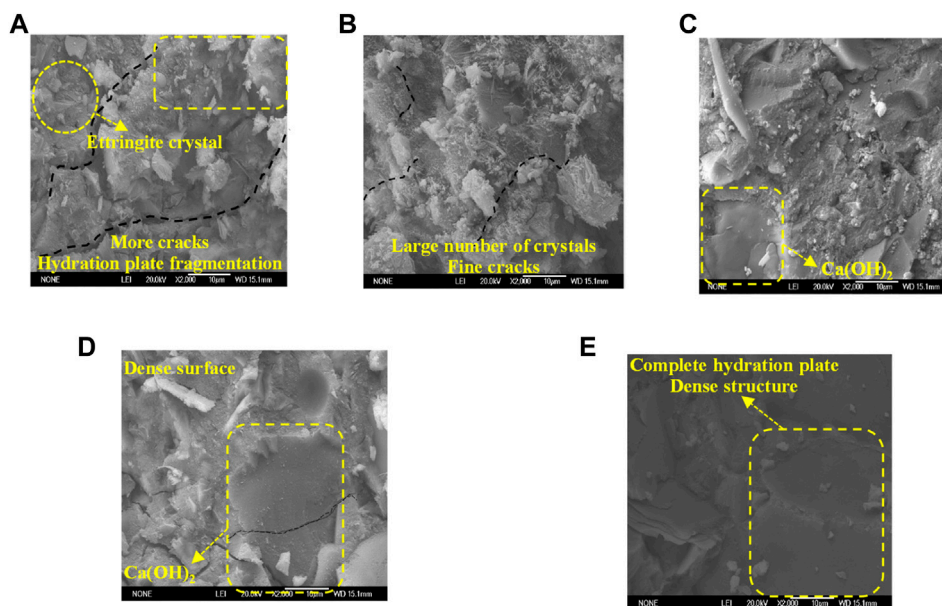


FIGURE 4 Microscopic scanning photos after 240 d of erosion (2000×). (A) Microscopic scanning image of S1 specimens. (B) Microscopic scanning image of S2 specimens. (C) Microscopic scanning image of S3 specimens. (D) Microscopic scanning image of S4 specimens. (E) Microscopic scanning image of S5 specimens.

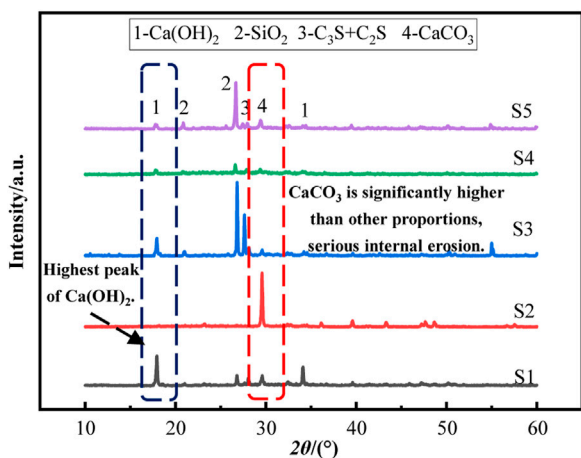


FIGURE 5 XRD patterns of each ratio before erosion.

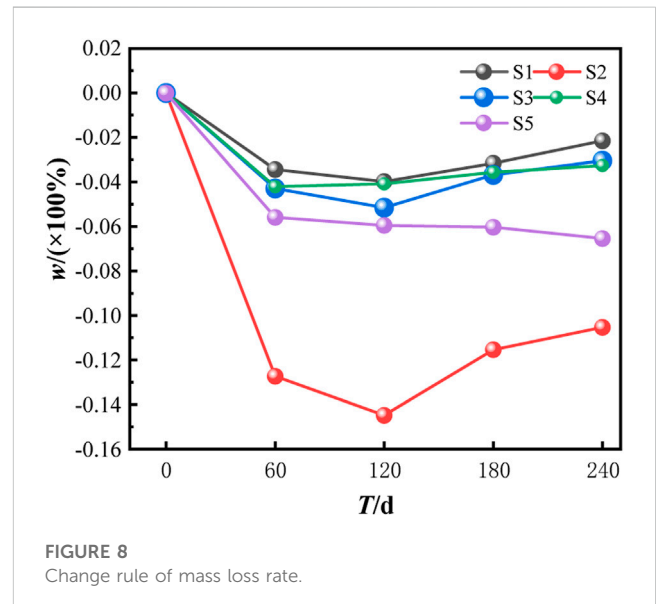
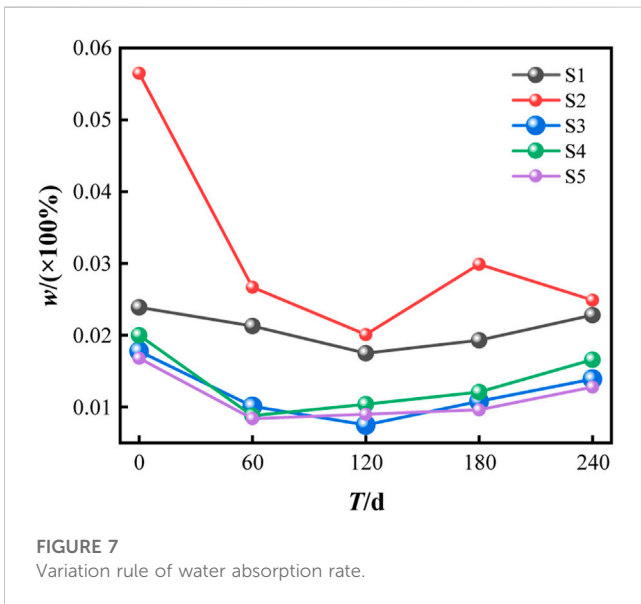
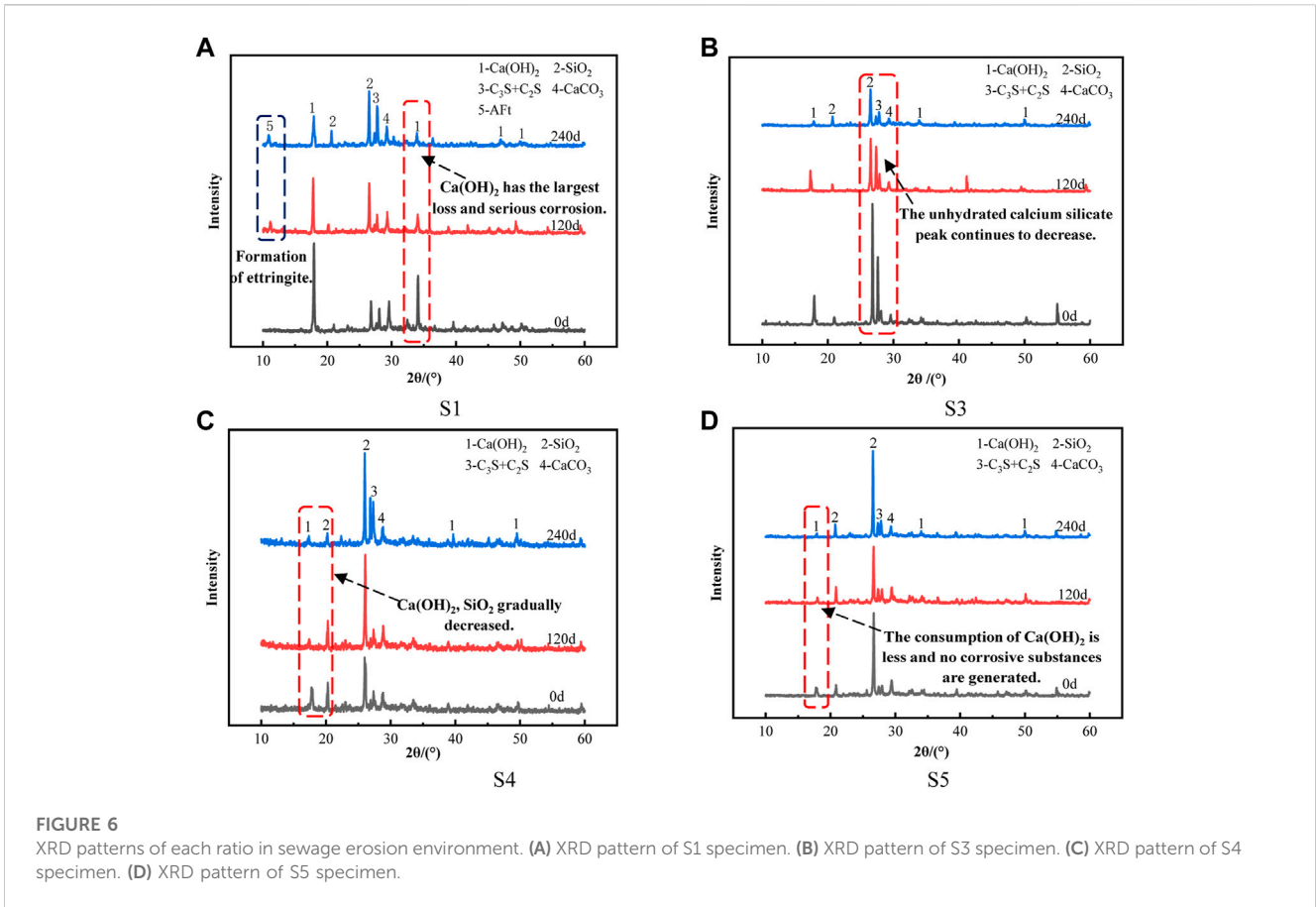
the generation of aggressive substances and improves the material’s corrosion resistance. It was found by the unhydrated calcium silicate peak that the peaks all occurred to a certain degree of increase. The peak was found by the unhydrated calcium silicate peak, which showed that the material could not continue to hydrate in the sewage erosion environment. There was a certain degree of internal damage, but the peak decreased in S3, indicating that adding sodium methyl silicate water repellent can continue to hydrate in late erosion.

We can find that inorganic aluminum salt water repellent makes the hydration reaction inside the test block more complete; sodium methyl silicate hinders the hydration of cement to a certain extent in the early stage of erosion, but after erosion, sodium methyl silicate makes the mortar continue to hydrate inside, thus showing better corrosion resistance. In the erosion environment, only S1 generated aggressive material ettringite, indicating that the mineral admixture and water repellent can reduce the generation of erosion material, effectively improving the material’s durability.

4.4 Water absorption and mass loss rate

The variation law of water absorption of each test block is shown in Figure 7. Before erosion, the water absorption rate of polymer mortar (S2) is as high as 5.65%, which is significantly higher than that of other ratios, and S3-S5 is not much different and lower. After 120 days of erosion, the water absorption rate all occurred in different degrees, among which S2 decreased the most, but the water absorption rate was still high; S3-S5 had the lowest water absorption rate. With the increase of the erosion cycle, the water absorption rate of each mixture ratio showed a trend of decreasing first and then increasing. After 240 d of erosion, the water absorption rate of S3-S5 specimens was significantly lower than that of S1 and S2. Among them, the minimum water absorption rate of S5 was only 55.46% of that of S2. The analysis shows that mineral admixtures and waterproofing agents can increase the density of mortar and reduce water absorption. Sodium methyl silicate and inorganic aluminum salt waterproof agent have the best effect.

The water absorption rate of the specimens after S2 erosion fluctuated greatly, showing the trend of drop-lift-drop. The increase



in specimen density is caused by the deposition of eroded material, which can fill the pores in the short term but can cause some damage to the internal structure. Since S2 produces more crystals and has not yet caused severe inner deterioration, the water absorption rate decreases significantly. S4, S5 in the erosion of 60 days when the

lowest water absorption rate, the rest of the test block erosion 120 days before the water absorption rate began to occur after the rise; indicate that the new anti-corrosion mortar erosion of less material, inorganic aluminum salt waterproofing agent for mortar corrosion resistance to enhance the role of obvious.

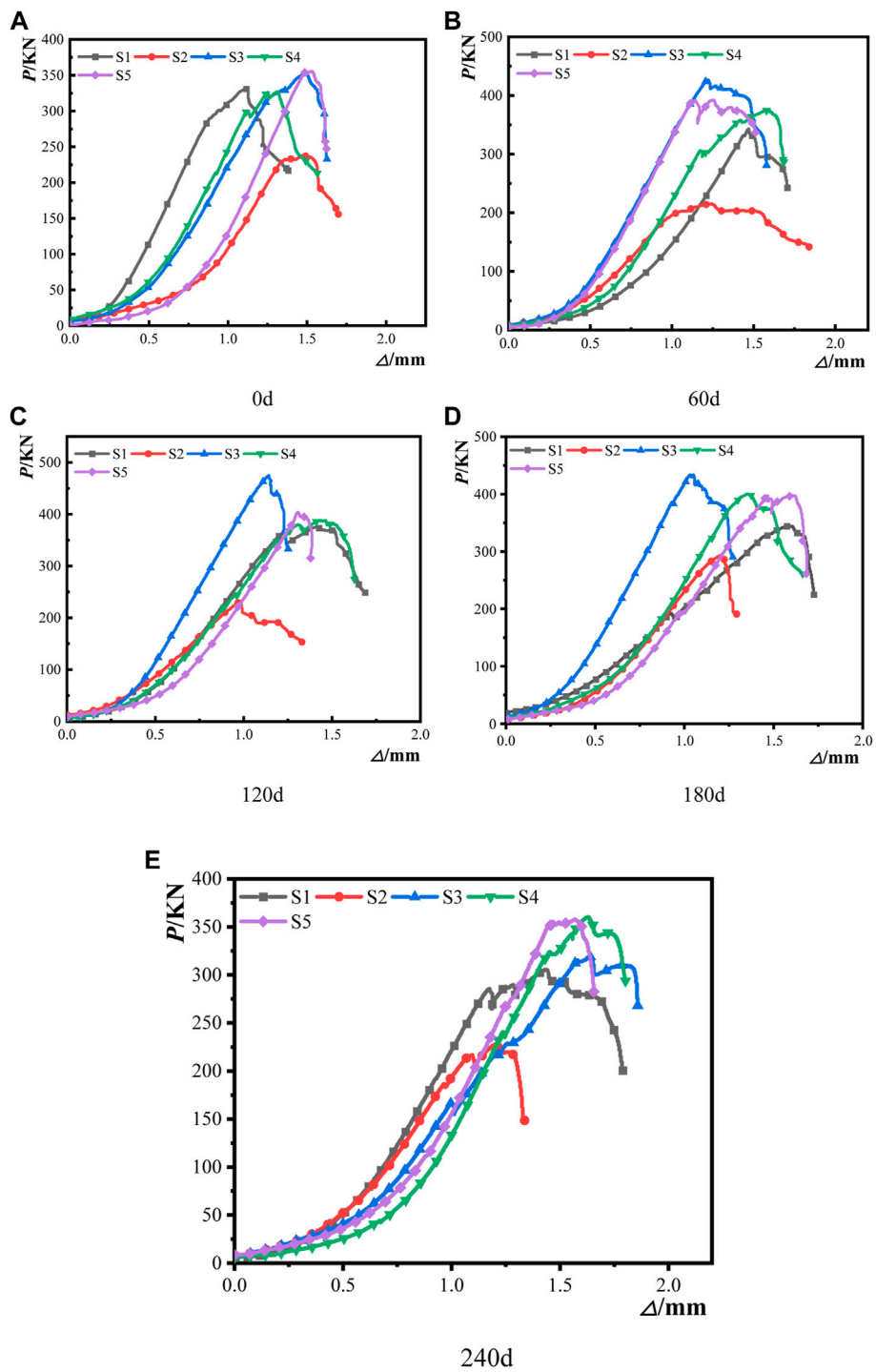
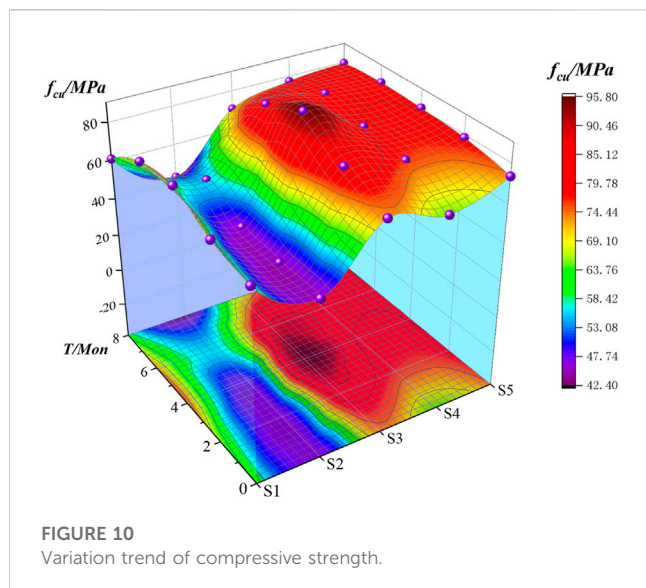


FIGURE 9 Load-settlement curve. (A) The load-settlement curve of S1 specimen. (B) The load-settlement curve of S2 specimens. (C) The load-settlement curve of S3 specimens. (D) The load-settlement curve of S4 specimens. (E) The load-settlement curve of S5 specimens.

According to the variation of mass loss rate in Figure 8, the quality of each proportion of mortar did not lose compared with the initial quality. With the increase in the erosion cycle, the quality loss rate of each mortar showed a trend of increasing and then decreasing. And the mass of S2 increases the most. According to the analysis, it is caused by the filling of pores by the erosion material

inside the mortar. In addition, the quality loss rate of each test block showed a relatively large fluctuation in an increasing trend, indicating that different degrees of damage occurred inside the mortar. Among them, S2 fluctuates the most, compared to S4 and S5 which have relatively stable quality after 60 days erosion, less internal damage and better overall performance.



In a comprehensive view, S1 has a high water absorption rate and mass loss rate, and S2 has a large number of internal crystals and the largest water absorption rate, both with poor performance. The water absorption and mass loss rate of S3-S5 are relatively low, indicating that the internal structure of the mortar is dense and no severe deterioration occurs. In general, adding a waterproof agent can effectively improve the density of the material, reduce water absorption, and improve durability to a certain extent.

4.5 Load displacement curve

Figure 9 shows the compressive load-displacement curves of each test block before and after erosion. As can be seen from the figure, the peak strength of the double-doped fiber mortar (S1) is substantially higher than that of the polymer mortar (S2) at all stages, indicating that the two fibers have a certain pulling effect within the material and effectively improve the mechanical properties of the material. Compared with S1, the peak strength of the ratio of sodium methyl silicate to inorganic aluminum salt (S3-S5) is further improved, indicating that adding mineral admixtures can effectively fill the pores and improve the compressive strength. After reaching the peak strength, the strength of S4 and S5 will decrease after 180 d of erosion, while the strength of the other ratios decreases after 120 d of erosion. Compared to S4, the S5 strength decline rate is slower, indicating that sodium methyl silicate and inorganic aluminum salt water repellent have excellent corrosion resistance. The S2 strength of the control group reached its peak material strength at about 25 MPa, while the strength of the fit ratio with added fibers was all higher. The crack-pulling action of the fibers enabled the load to continue to rise even after cracks appeared in the test blocks. Qin et al. (2018) found that the reinforcing effect of the fibers was more prominent after the material cracking.

Overall, each mortar test block showed good performance in the early stage, and the strength of each ratio decreased to some extent with the increase of the erosion cycle. This is mainly because the mortar is slightly eroded at the beginning, the internal can continue

TABLE 3 Compressive strength of each specimen (unit:MPa).

Erosion time (d)	S1	S2	S3	S4	S5
0	63.02	45.38	72.96	64.47	73.58
60	67.23	45.39	82.32	76.24	78.53
120	77.26	46.75	95.01	79.18	80.27
180	74.19	55.71	85.61	83.10	81.02
240	61.28	42.56	70.52	77.23	79.45

to hydrate, and the test block can maintain a high strength; with the intensification of erosion, the test block's internal generation of calcium alumina and other expansive erosion material, long-term accumulation will lead to the test block internal damage, resulting in a continuous decrease in material strength.

4.6 Variation trend analysis of compressive strength

Figure 10 is the trend chart of the compressive strength of each mix proportion. The overall strength of each ratio is increasing first and then decreasing trend, and the pore space is decreasing first and then increasing trend basically coincides, indicating that the porosity and strength are negatively correlated; the higher the porosity, the lower the high strength. Combined with Table 3, it is found that the strength of S2 at 0 days is significantly lower than that of the other mix proportions. The initial strength of S3-S5 is more than 1.4 times higher than that of S2, indicating that the admixture can improve the compactness and the material's mechanical properties. After 240 d of erosion, S3-S5 continued to maintain good performance. The strength retention rate of S4 reached 119.79%, and the residual strength was 77.23 MPa, nearly 30% higher than that of S2, and the residual strength was increased by more than 80%. It can be seen that an inorganic aluminum salt waterproofing agent can slow down the rate of strength decline and significantly improve the corrosion resistance of mortar.

In summary, fiber can improve materials' toughening and crack resistance and effectively improve materials' mechanical properties. Mineral admixture can improve the dense property and increase the compressive strength. The addition of sodium methyl silicate and inorganic aluminum salt waterproofing agents can effectively slow down the strength decay rate and improve corrosion resistance.

4.7 Injury mechanism and protection principle

Through the above test results of different ratio test block macro and microstates, we found that sodium methyl silicate and inorganic aluminum salt waterproofing agent to enhance the mortar test block in the harsh environment corrosion resistance has a significant effect on the material damage mechanism and waterproofing agent protection principle is as follows.

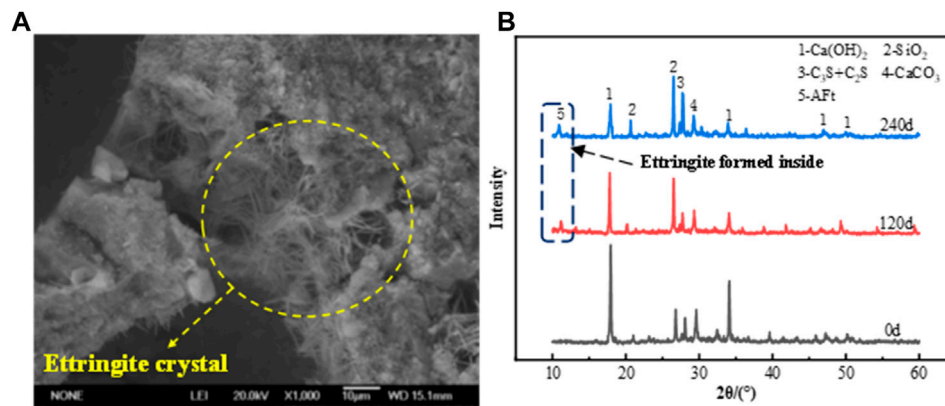


FIGURE 11 SEM (A) and XRD (B) patterns of eroded materials.

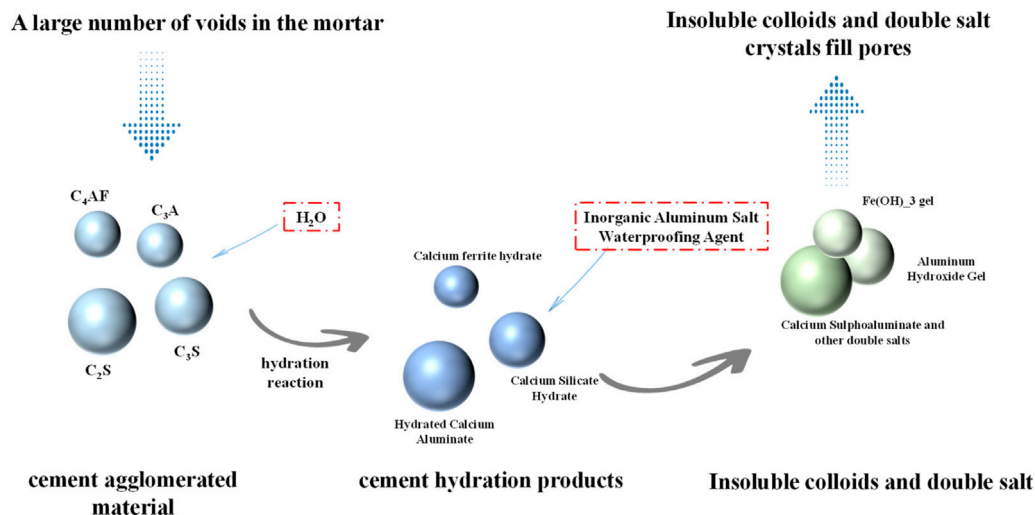
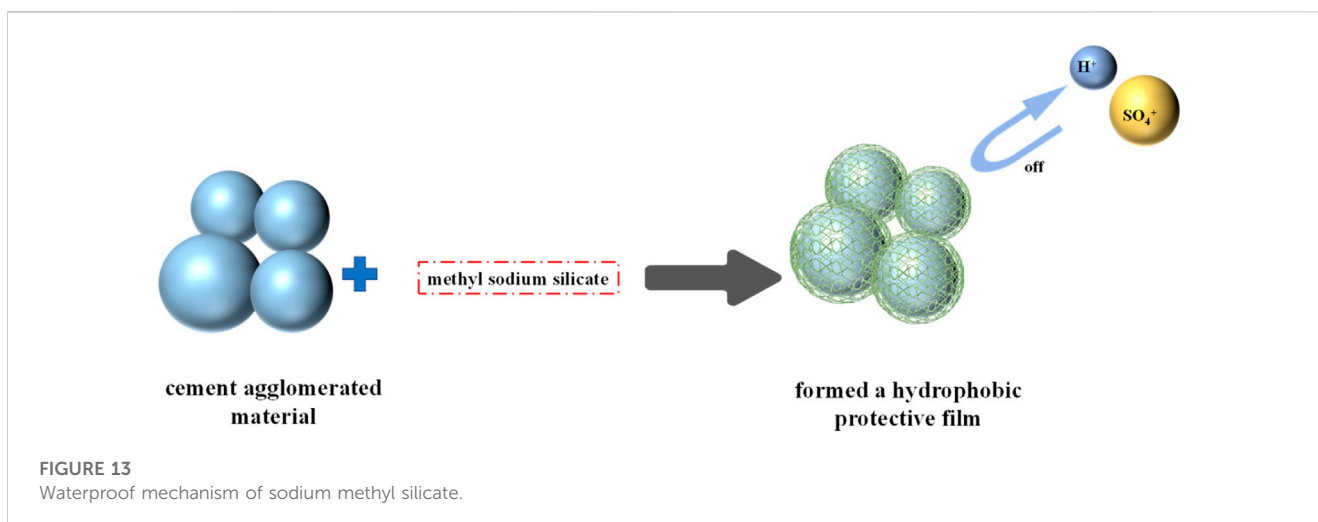


FIGURE 12 Protective mechanism of inorganic aluminum salt waterproofing agent.

Currently, it is generally believed that the corrosion of the sewage environment is caused by microbial metabolism and acid production. In a humid climate, the alkaline substances generated by hydration in cement-based materials will carbonize with carbon dioxide and water, resulting in a continuous decrease in the alkalinity of the material and a decrease in the pH value, which provides conditions for microbial reproduction. SO_4^{2-} in the sludge is reduced by sulfate-reducing bacteria (SRB) to produce H_2S gas, which reacts with bacteria to produce biological sulfuric acid (Hendi et al., 2017; Georgios et al., 2021). Various acids such as biological sulfuric acid and organic acid produced by microbial metabolism are continuously accumulated and infiltrated. Over time this will increase the water absorption and permeability of the material and lead to the degradation of mechanical properties. Sulfate ions are targeted damage caused by the directional attraction of calcium ions through biofilm pores in an electrical manner, thus causing severe damage to the structure. In addition, cement-based materials will react with biological sulfuric acid

to form expansive materials such as gypsum and ettringite to fill pores (Figure 11), reducing the structural strength, increasing the porosity, and eventually leading to the cracking of the structure.

The study found that adding a waterproofing agent can fill the internal pores and reduce the water absorption of the material, which significantly improves the corrosion of structures in harsh environments. Among them, inorganic aluminum salt waterproofing agent and cement-based materials in the cement hydration products (hydrated calcium ferrate, hydrated calcium aluminate, hydrated calcium silicate) reaction to generate insoluble colloids and expansion-type compound salt crystals to fill the pores and increase the material density, its mechanism of action see Figure 12 sodium methyl silicate as a new construction waterproofing agent, in the action of water and carbon dioxide will generate methyl silicate alcohol. Methyl silicate alcohol further cement-based material reaction, in the structure of the material surface and the internal generation of a few molecules thick water



repellent network membrane, it can block the ion penetration and thus greatly improve the material impermeability, its mechanism of action in Figure 13. The test found that the addition of sodium methyl silicate and inorganic aluminum salt waterproofing agent can effectively reduce the number of internal open pores, increase the density of the material, the formation of a rigid waterproof layer, blocking the penetration of harmful ions, which can slow down the rate of material strength decay, and significantly improve the corrosion resistance of the material. The analysis of the experimental results of cement-based material erosion lays a foundation for future machine learning and residual life prediction after material corrosion (Huang et al., 2020b; Huang et al., 2020c; Chang et al., 2020; Medina et al., 2021).

On the whole, the fiber can improve the internal compactness of mortar, blocking harmful ion transfer paths. Methyl sodium silicate can form a water-repellent film with low tension on the pore surface to reduce ion penetration. Insoluble colloids produced by inorganic aluminum salts can fill the pores and increase their density. On balance, inorganic aluminum salts are the most effective and are recommended for priority use.

5 Conclusion

This paper studies the durability of new anti-corrosion mortar in an erosion environment. The main conclusions are as follows:

- (1) Mortar surface will produce many crystals and brownish-black algae deposition after erosion. The erosion of mortar mixed with sodium methyl silicate and inorganic aluminum salt waterproofing agent is obviously reduced. This new mortar significantly improves compactness and water absorption over ordinary fiber and polymer mortars.
- (2) From the microscopic point of view found that ordinary polymer mortar test blocks are loose and porous. Adding admixtures and waterproof agents to mortar will make its internal pores less and hydration hardening complete. The apparent compactness of mortar is the best after adding sodium methyl silicate and inorganic aluminum salt waterproofing agent.

- (3) The initial strength of the new mortar is higher, reaching more than 60 MPa. It is more than 40% stronger than the current mainstream polymer mortar. There are fewer cracks after compression failure, showing good mechanical properties. After sewage corrosion, the strength of polymer mortar is reduced by nearly 6%, and the strength of high corrosion-resistant mortar is increased by 20%, showing excellent corrosion resistance. On balance, inorganic aluminum salts are the most effective and are recommended for priority use.
- (4) Applying the impermeability of sodium methyl silicate and the ability of inorganic aluminum salt waterproofing agent to fill pores in cement-based materials to construction materials can effectively improve the service life of structures and provide support for structural engineering repair and protection in complex corrosive environments.

Data availability statement

The original contributions presented in the study are included in the article/supplementary material, further inquiries can be directed to the corresponding author.

Author contributions

Conceptualization, JW and ZW; methodology, JX and HJ; software, ZW; validation, JX and HJ; investigation, JW and ZW; resources, JW and ZW; data curation, JX and HJ; writing—original draft preparation, JW, ZW, JX and HJ; writing—review and editing, ZW; visualization, JW and ZW; supervision, JW; funding acquisition, JW; project administration, JW.

Conflict of interest

The authors declare that the research was conducted in the absence of any commercial or financial relationships that could be construed as a potential conflict of interest.

Publisher's note

All claims expressed in this article are solely those of the authors and do not necessarily represent those of their affiliated

organizations, or those of the publisher, the editors and the reviewers. Any product that may be evaluated in this article, or claim that may be made by its manufacturer, is not guaranteed or endorsed by the publisher.

References

- Afroz, M., Patnaikuni, I., and Venkatesan, S. (2017). Chemical durability and performance of modified basalt fiber in concrete medium. *Constr. Build. Mat.* 154, 191–203. doi:10.1016/j.conbuildmat.2017.07.153
- Alkharabshah, B. N., Arbili, M. M., Majidi, A., Alogla, S. M., Hakamy, A., Ahmad, J., et al. (2022). Basalt fibers reinforced concrete: Strength and failure modes. *Mater* 15 (20), 7350. doi:10.3390/MA15207350
- Bahtli, T., and Ozbay, N. S. (2020). Corrosion resistances of C30 concrete: Effect of finely ground bronze sawdust waste. *Mat. Chem. Phys.* 243 (C), 122588. doi:10.1016/j.matchemphys.2019.122588
- Chang, Z., Du, Z., Zhang, F., Huang, F., Chen, J., Li, W., et al. (2020). Landslide susceptibility prediction based on remote sensing images and GIS: Comparisons of supervised and unsupervised machine learning models. *Remote Sens.* 12, 502. doi:10.3390/rs12030502
- Chen, L. L., Wang, Y. Q., Wang, Z. F., Chang, H. T., and Fan, F. F. (2022). Diffusion resisting performance of concrete modified with sodium methyl silicate in saline soil area. *Constr. Build. Mat.* 350, 128767. doi:10.1016/j.conbuildmat.2022.128767
- Danuta, B. -H., Grzegorz, L., Stanisław, F., and Jarosz-Hadam, M. (2018). Effect of polysiloxanes on roughness and durability of basalt Fibres Reinforced cement mortar. *Polym* 10 (4), 420. doi:10.3390/polym10040420
- Elgabbas, F., Vincent, P., Ahmed, E. A., and Benmokrane, B. (2016). Experimental testing of basalt-fiber-reinforced polymer bars in concrete beams. *Compos. Part B* 91, 205–218. doi:10.1016/j.compositesb.2016.01.045
- Fiore, V., Calabrese, L., Bella, G. D., Scalici, T., Galtieri, G., Valenza, A., et al. (2016). Effects of aging in salt spray conditions on flax and flax/basalt reinforced composites: Wettability and dynamic mechanical properties. *Compos. Part B* 93, 35–42. doi:10.1016/j.compositesb.2016.02.057
- Gao, S., Ji, Y., Qin, Z. W., Zhang, H. W., Xing, F., and Liu, A. (2022). A comprehensive analysis of pore structures and performances of mineral admixtures modified recycled aggregate concrete based on experiment and theory. *Constr. Build. Mat.* 358, 129451. doi:10.1016/j.conbuildmat.2022.129451
- Georgios, F., Anastasios, T., Costas, A. A., Efthimios, P., and Petros, S. (2021). The inclusion of acidic and stormwater flows in concrete sewer corrosion mitigation studies. *Water* 13 (3), 261. doi:10.3390/W13030261
- Guo, Z. Z., Chen, L. X., Yin, K. L., Shrestha, D. P., and Zhang, L. (2020). Quantitative risk assessment of slow-moving landslides from the viewpoint of decision-making: A case study of the three gorges reservoir in China. *Eng. Geol.* 273, 105667. doi:10.1016/j.enggeo.2020.105667
- Hendi, A., Behravan, A., Mostofinejad, D., Moshtaghi, S. M., and Rezayi, K. (2017). Implementing ANN to minimize sewage systems concrete corrosion with glass beads substitution. *Constr. Build. Mat.* 138, 441–454. doi:10.1016/j.conbuildmat.2017.02.034
- Huang, F., Cao, Z. S., Guo, J. F., Jiang, S. -H., and Guo, Z. Z. (2020a). Comparisons of heuristic, general statistical and machine learning models for landslide susceptibility prediction and mapping. *CATENA* 191, 104580. doi:10.1016/j.catena.2020.104580
- Huang, F., Cao, Z. S., Jiang, S. -H., Zhou, C. B., and Guo, Z. Z. (2020c). Landslide susceptibility prediction based on a semi-supervised multiple-layer perceptron model. *Landslides* 17, 2919–2930. doi:10.1007/s10346-020-01473-9
- Huang, F., Zhang, J., Zhou, C. B., Wang, Y. H., Huang, J. S., and Zhu, L. (2020b). A deep learning algorithm using a fully connected sparse autoencoder neural network for landslide susceptibility prediction. *Landslides* 17 (01), 217–229. doi:10.1007/s10346-019-01274-9
- Huber, B., Hilbig, H., Mago, M. M., Drewes, J. E., and Müller, E. (2016). Comparative analysis of biogenic and chemical sulfuric acid attack on hardened cement paste using laser ablation-ICP-MS. *Cem. Concr. Res.* 87, 14–21. doi:10.1016/j.cemconres.2016.05.003
- Izquierdo, S., Diaz, J., de Gutiérrez, R. M., and Torres, A. J. (2016). Durabilidad de morteros adicionados con FCC expuestos a sulfato de magnesio y sulfato de sodio. *Rev. Ing. Construcción*. 31 (3), 183–190. doi:10.4067/S0718-50732016000300004
- Jensen, H. S., Lens, P. N. L., Nielsen, J. L., Bester, K., Nielsen, A. H., Thorkild, H. -J., et al. (2011). Growth kinetics of hydrogen sulfide oxidizing bacteria in corroded concrete from sewers. *J. Hazard. Mat.* 189 (3), 685–691. doi:10.1016/j.jhazmat.2011.03.005
- Jiang, S. H., Huang, J., Huang, F. M., Yang, J. H., Yao, C., and Zhou, C. B. (2020). Modelling of spatial variability of soil undrained shear strength by conditional random fields for slope reliability analysis. *Appl. Math. Modell.* 63, 374–389. doi:10.1016/j.apm.2018.06.030
- Kallel, T., Kallel, A., and Samet, B. (2016). Durability of mortars made with sand washing waste. *Constr. Build. Mat.* 122, 728–735. doi:10.1016/j.conbuildmat.2016.06.086
- Li, X. G., Ma, Q. G., Ji, Y. F., Cheng, K. D., and Sun, Z. L. (2022). Study on the improvement of waterproof performance of historical silt sites with silicone waterproofing agent. *Coat.* 12 (8), 1162. doi:10.3390/COATINGS12081162
- Li, X., O'Moore, L., Song, Y. R., Bond, P. L., Yuan, Z., Wilkie, S., et al. (2019). The rapid chemically induced corrosion of concrete sewers at high H₂S concentration. *Water Res.* 162, 95–104. doi:10.1016/j.watres.2019.06.062
- Lukowski, P., and Dębska, D. (2019). Effect of polymer addition on performance of Portland cement mortar exposed to sulphate attack. *Mater* 13 (1), 71. doi:10.3390/ma13010071
- Ma, A. J., Li, Z. S., and Feng, X. R. (2021). Experimental study on performance of fiber concrete under simulated acid rain environment. *IOP Conf. Ser. Earth Environ. Sci.* 787 (1), 012010. doi:10.1088/1755-1315/787/1/012010
- Ma, Q. W., Liu, Q., Cheng, K. D., and Liu, S. (2022). Study on the durability of hydraulic lime soil mixed with sodium methyl silicate. *Coat* 12 (7), 903. doi:10.3390/coatings12070903
- Mahdikhani, M., Bamshad, O., and Shirvani, M. F. (2018). Mechanical properties and durability of concrete specimens containing nano silica in sulfuric acid rain condition. *Constr. Build. Mat.* 167, 929–935. doi:10.1016/j.conbuildmat.2018.01.137
- Medina, V., Hürlimann, M., Guo, Z. Z., Lloret, A., and Vaunat, J. (2021). Fast physically-based model for rainfall-induced landslide susceptibility assessment at regional scale. *Catena* 201, 105213. doi:10.1016/j.catena.2021.105213
- Negar, R., and Nemkumar, B. (2021). An innovative approach to simulate biocorrosion in concrete pipes. *J. Test. Eval.* 49 (2), 20180642. doi:10.1016/j.proeng.2013.09.051
- Nehdi, M. L., Suleiman, A. R., and Soliman, A. M. (2014). Investigation of concrete exposed to dual sulfate attack. *Cem. Concr. Res.* 64, 42–53. doi:10.1016/j.cemconres.2014.06.002
- Noeiaghaj, T., Mukherjee, A., Dhami, N., and Chae, S. R. (2017). Biogenic deterioration of concrete and its mitigation technologies. *Constr. Build. Mater* 149, 575–586. doi:10.1016/j.conbuildmat.2017.05.144
- Pandey, A., and Kumar, B. (2020). Investigation on the effects of acidic environment and accelerated carbonation on concrete admixed with rice straw ash and microsilica. *J. Build. Eng.* 29 (C), 101125. doi:10.1016/j.jobte.2019.101125
- Qin, J. H., Qian, J. S., Li, Z., You, C., Dai, X., and Yue, Y. F. (2018). Mechanical properties of basalt fiber reinforced magnesium phosphate cement composites. *Constr. Build. Mat.* 188, 946–955. doi:10.1016/j.conbuildmat.2018.08.044
- Quagliarini, E., Monni, F., Bondioli, F., and Lenci, S. (2015). Basalt fiber ropes and rods: Durability tests for their use in building engineering. *J. Build. Eng.* 5, 142–150. doi:10.1016/j.jobte.2015.12.003
- Ralegaonkar, R., Gavali, H., Aswath, P., and Abolmaali, S. (2018). Application of chopped basalt fibers in reinforced mortar: A review. *Constr. Build. Mat.* 164 (10), 589–602. doi:10.1016/j.conbuildmat.2017.12.245
- Schneider, M. (2015). Process technology for efficient and sustainable cement production. *Cem. Concr. Res.* 78, 14–23. doi:10.1016/j.cemconres.2015.05.014
- Song, Y. R., Tian, Y. M., Li, X., Wei, J., Zhang, H. Y., Bond, P. L., et al. (2018). Distinct microbially induced concrete corrosion at the tidal region of reinforced concrete sewers. *Water Res.* 150, 392–402. doi:10.1016/j.watres.2018.11.083
- Sun, X. Y., Jiang, G. M., Bond, P. L., and Keller, J. (2019). Periodic deprivation of gaseous hydrogen sulfide affects the activity of the concrete corrosion layer in sewers. *Water Res.* 157, 463–471. doi:10.1016/j.watres.2019.03.074
- Wang, T., Wu, K., Kan, L. L., and Wu, M. (2020a). Current understanding on microbially induced corrosion of concrete in sewer structures: A review of the evaluation methods and mitigation measures. *Constr. Build. Mat.* 247, 118539. doi:10.1016/j.conbuildmat.2020.118539
- Wang, T. Y., Zhang, D., Zhu, H., Ma, B., and Li, V. C. (2022). Durability and self-healing of engineered cementitious composites exposed to simulated sewage environments. *Cem. Concr. Compos.* 129, 104500. doi:10.1016/j.cemconcomp.2022.104500
- Wang, X., Jiang, L., Shen, H., and Wu, Z. S. (2018). Long-term performance of pultruded basalt fiber reinforced polymer profiles under acidic conditions. *J. Mat. Civ. Eng.* 30 (6), 04018096. doi:10.1061/(asce)mt.1943-5533.0002293
- Wang, Y., Zhang, S. H., Niu, D. T., Su, L., and Luo, D. (2020b). Strength and chloride ion distribution brought by aggregate of basalt fiber reinforced coral aggregate concrete. *Constr. Build. Mat.* 234, 117390–117411. doi:10.1016/j.conbuildmat.2019.117390

Wang, Z. S., Li, Y. K., Lu, J. L., Bao, T. J., and Zhao, K. (2020c). Research on corrosion characteristics and performance degradation of basalt fiber concrete under sodium magnesium sulfate corrosion environment. *J. Coast. Res.* 111 (1), 56–62. doi:10.2112/JCR-SI111-010.1

Wu, M., Wang, T., Wu, K., and Kan, L. L. (2020). Microbiologically induced corrosion of concrete in sewer structures: A review of the mechanisms and phenomena. *Constr. Build. Mater.* 239 (C), 117813. doi:10.1016/j.conbuildmat.2019.117813

Xiang, T. F., Liu, J., Lv, Z., Wei, F., Liu, Q., Zhang, Y., et al. (2021). The effect of silicon-based waterproof agent on the wettability of superhydrophobic concrete and enhanced

corrosion resistance. *Constr. Build. Mat.* 313, 125482. doi:10.1016/J.CONBUILDMAT.2021.125482

Xu, J., Tang, Y. H., Wang, X. Z., Wang, Z. P., and Yao, W. (2020). Application of ureolysis-based microbial CaCO_3 precipitation in self-healing of concrete and inhibition of reinforcement corrosion. *Constr. Build. Mat.* 265, 120364. doi:10.1016/j.conbuildmat.2020.120364

Zhang, C. Y., Liu, T. Y., Jiang, C., Zhao, C., Zhou, K. P., and Chen, L. J. (2022). The freeze-thaw strength evolution of fiber-reinforced cement mortar based on NMR and fractal theory: Considering porosity and pore distribution. *Mat.* 15 (20), 7316. doi:10.3390/MA15207316